PERGAMON

Computers & Fluids 29 (2000) 467–492

computers & fluids

www.elsevier.com/locate/compfluid

Side wall effects on the structure of laminar flow over a plane-symmetric sudden expansion

T.P. Chiang, Tony W.H. Sheu*, S.K. Wang

Department of Naval Architecture and Ocean Engineering, National Taiwan University, 73 Chou-Shan Rd. Taipei, Taiwan

Received 29 June 1998; received in revised form 29 April 1999; accepted 29 April 1999

Abstract

Computational investigations have been performed in order to study the side-wall effect on a fluid downstream of a channel expansion which is plane. The expansion ratio under investigation is 3 and the aspect ratios are 3, 3.5, 3.75, 4, 5, 6, 7, 8, 9, 10, 12, 18, 24, 48, in the three-dimensional analyses. For the flow with a value of $Re = 60$, results show symmetric nature of the flow when the channel aspect ratio has a value less than 3.5. Beyond this critical aspect ratio, flow symmetry can no longer be sustained due to the Coanda effect. This confirms the experimental observation that a decrease in aspect ratio has a stabilizing effect. Unless the aspect ratio is increased further to a value above 12, flow in the third dimension plays an essential role to characterize the inherent nature of the flow. In this study, we also confine ourselves to studying flow separation, reattachment, and recirculation by employing a theoretically rigorous theory of topology. Much insight into the vortical flow structure can be revealed from limiting streamlines, on which critical points, such as spiral focal points and saddles, are plotted.

1. Introduction

It is well known that a flow through a channel with sudden expansion about its centerline becomes asymmetric as the Reynolds number increases. This is often referred to as the Coanda effect in the literature [1]. In mathematical terms, bifurcation occurs when multiple stable

* Corresponding author. Tel.: +886-2-3625470 ext. 246; fax: +886-2-23929885.
E-mail address: sheu@indy.na.ntu.edu.tw (T.W.H. Sheu).

0045-7930/00/$ - see front matter
PII: S0045-7930(99)00018-3

solutions to Navier–Stokes equations exist [2]. The origin of such steady asymmetric flow is due to an increase in velocity near one wall and the accompanying decrease in pressure near that wall; once the resulting pressure difference is established across the channel, flow asymmetry is maintained. No physically rigorous explanations for this flow asymmetry have been presented. Cherdron et al. [3] attributed these instabilities to disturbances generated in the step corner of expansion, which are amplified in the shear layer. In 1985, Sobey further confirmed the asymmetric disturbance, configured in a vortex sheet, in the experiment [4]. A better understanding of such shear-layer related instability in the sudden-expansion channel flow is important to provide a basis for understanding the pitchfork bifurcation in a high Reynolds number flow and the presence of Hopf bifurcation in a time-periodic flow [2].

There have been extensive studies of this problem in the literature. One can explore into flow bifurcation analytically by applying the bifurcation theory [2,5–7]. An observation common to many of other flow studies is that the solution remains unique at sufficiently low Reynolds numbers. Sobey and Drazin [2] clarified the possibility of observing multiple stable solutions in the channel flow using bifurcation theory. They also demonstrated that the unique symmetric flow which exists at small Re is not stably maintained at larger Re due to the presence of a pitchfork bifurcation. The emergence of two stable asymmetric flows is indicative of the occurrence of such bifurcation. As the value of Re is increased further, the flow may evolve in two ways. One possibility is that the steady two-dimensional asymmetric solutions will become unstable. Under the circumstances, flow in the third dimension becomes prevailing. There exists another type of bifurcation, known as the Hopf bifurcation, which may result in a time-periodic solution. Our purpose here is not to study the Coanda effect using bifurcation theory. Thus, we have no intention to provide an exhaustive list of references to this subject, but rather to point to two most recently published papers [8,9], which may provide additional information on this topic.

Many experimental investigations have also been performed on this problem, for instance, by Macagno and Hung [10], Durst et al. [11], Cherdron et al. [3], Sobey [4], Sobey and Drazin [2], Fearn et al. [5], and Durst et al. [12]. The main results are that in a channel of symmetric geometry, the symmetric flow becomes unstable as the Reynolds number exceeds the critical value. The critical Reynolds number depends strongly on the expansion ratio, E, as well as on the aspect ratio, A, of the channel [3]. They experimentally confirmed the Coanda effect which causes the flow attached to one wall to have a higher velocity and, thus, a lower pressure; as a result, the asymmetric flow can be stably maintained by the cross-channel pressure gradient. One point worth addressing is that the flow over a backward-facing step is a special case of this class of experimental work [13].

There have also been considerable numerical investigation of sudden-expansion flow. Much of the previous work has been directed towards two-dimentional simulation of Navier–Stokes equations [4–7,10,12,14]. These computational studies have revealed the general trends of previous experimental observations. Under high Reynolds number conditions, experimental observation has shed new light on the inappropriate use of the two-dimentional assumption in numerical investigation of the expansion flow into the channel. In recent years, significant progress has made three-dimensional Navier–Stokes flow simulations possible. To make full use of the available power, we can provide information which adds to the knowledge of the flow structure through analysis of higher Reynolds number flows in three dimensions. This is

the motivation for the present paper. The flow configuration we use in our study is that of an idealized expansion of Fearn et al. [5] in order to allow comparison of the predicted and experimental results. We present steady-state solutions for $Re = 60$ and 140 in the channel with a fixed value of the expansion ratio E ($\equiv 3$). In this study, we also pay special attention to how the side wall can affect the flow asymmetry in expansion channels with different aspect ratios.

The remainder of the paper is divided into four sections. Section 2 describes the mathematical model, which represents the conservation of mass and momentum for the incompressible fluid flow. This is followed by presentation of the numerical model used to solve the steady Navier–Stokes equations, subject to proper boundary conditions, in three dimensions. The results are discussed in the subsequent section and relevant flow topologies inferred from three-dimensional data are depicted. Finally, in Section 5, we make concluding remarks regarding the implications of the computed results.

2. Mathematical model

Computational modeling of channel flow requires, in the general case, solving three-dimensional transient flow equations. In this study, we concentrate on steady-state equations for a flow with a Reynolds number $Re < 150$. This steady-state assumption has been experimentally confirmed by Fearn et al. [5]. In rectangular coordinates, the relevant equations of motion which are constrained by the divergence-free incompressibility condition are posed

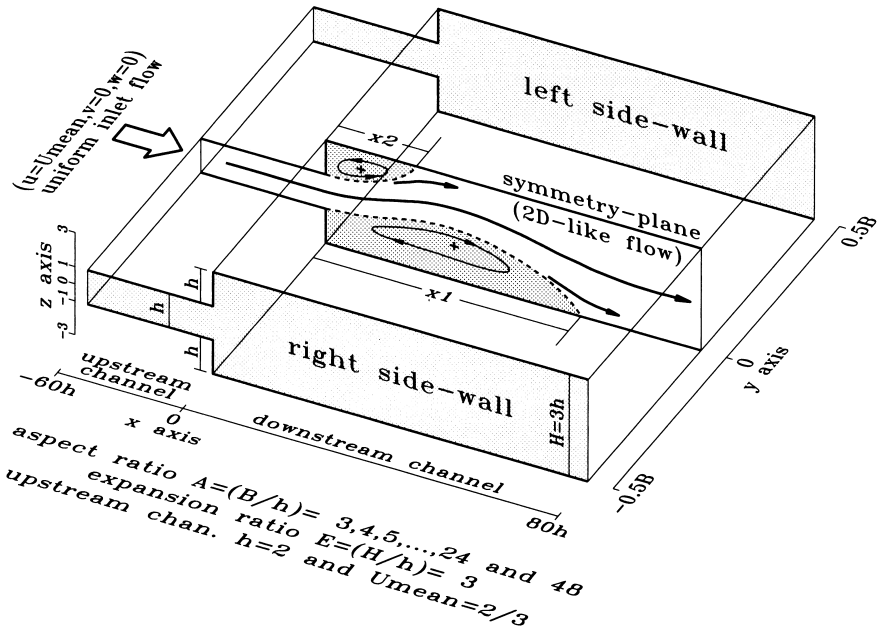

Fig. 1. The geometry and flow condition for the three-dimensional flow analysis in the plane-symmetric channel with sudden-expansion ratio $E = 3$.

as follows:

$$\underline{u} \cdot \nabla \underline{u} = -\nabla p + \frac{1}{Re} \nabla^2 \underline{u}, \tag{1}$$

$$\nabla \cdot \underline{u} = 0 \tag{2}$$

The above primitive variable formulation has advantages over formulations using vorticity-based variables where the research scientists are more acquainted with the physical meaning of velocity and pressure variables. This helps us explore the physics of a flow inferred directly from computed data. The other advantage of the primitive-variable formulation is the accommodation of the closure boundary condition [15].

The primitive variables adopted are made dimensionless by choosing half of the upstream channel height ($h = 2$), shown schematically in Fig. 1, as the reference length and 1.5 times of the mean velocity ($u_{\text{mean}} = 2/3$) prescribed over at the inlet of the upstream channel, which is 60 h ahead of the expansion plane. For this study, the Reynolds number of the flow is defined as $Re = (\frac{3}{2}u_{\text{mean}})(\frac{1}{2}h)/\nu$, where ν is known as the kinematic viscosity. For the present inflow–outflow problem to be mathematically well-posed, the working equations must be subject to boundary conditions. At the inlet plane, which is sufficiently distant from the expansion plane, we prescribe a flow with a uniform velocity vector (2/3, 0, 0). At the opposite end of the channel, we also assign boundary conditions. According to Fearn et al. [5], a length of 80 h is sufficient for the flow to develop fully again, thus allowing us to specify zero gradient conditions at the synthetic outlet. No-slip boundary conditions are prescribed on the solid wall of the channel.

3. Numerical model and code validation

We will now transform working equations into their discrete counterparts using a finite volume method so that they are amenable to computer simulation. Primitive variables are stored on staggered, interconnected grids, each of which is associated with a representative primitive variable [16]. Grid staggering prevents node-to-node pressure oscillations from arising in the approximation of pressure gradient terms. While considerable complexity is added to the programming effort, there is an advantage in the implementation of the boundary conditions on staggered grids. The main attribute of the formulation is that we can dispense with the pressure boundary condition along the boundary, where no storage points are given for the pressure.

A serious problem which was encountered while performing the flow analysis was the numerical diffusion error. As a remedy to this difficulty, a QUICK discretization scheme implemented on non-uniform grids [17] is considered as a refinement to Leonard's original scheme [18] for the spatial discretization. This upwind treatment of advective terms stabilizes the discrete system and provides a numerical scheme that is globally second-order accurate in space. Other spatial derivatives in the equations are approximated using a second-order accurate centered scheme.

In Eqs. (1) and (2), there is no explicit pressure equation which can be used to solve for the pressure field. The lack of an explicit pressure equation presents a serious computational difficulty in the mixed formulation. The difficulty lies in the loss of diagonal dominance and, thus, weakens the discrete system. The segregated approach, advocated by Patankar [19], is a well-known straightforward method for resolving this difficulty. In this study, we employ the pressure difference p' as a representative working variable to replace the continuity equation. The resulting Poisson equation for p' is used to compensate the pressure–velocity decoupling. As a direct consequence of this decoupling nature of the working equations, it is appropriate to apply the semi-implicit iterative algorithm. A substantial reduction in disk storage is the obvious benefit. In this study, we applied a semi-implicit solution algorithm, which is similar to the SIMPLE-C [20], to solve three momentum equations and one Poisson equation for the pressure difference in a cyclic predict-and-correct process. The details of this solution algorithm is as follows.

We start the calculation by setting the pressure values to zero. This is followed by solving three momentum equations to obtain their representative primitive velocities through introduction of under-relaxation E-factors to the discrete equations. We take larger E-factor for the prevailing velocity-component to speed-up the calculation. We also calculate the coefficients shown in the p'equation using the most updated velocities. When solving the Poisson equation for p', we carry out the calculation using an over-relaxation factor as high as 1.99. The solution for p' is obtained in an alternating-direction-implicit fashion. As is usual, 10 to 20 inner iterations are needed to obtain convergent p' solutions. Upon obtaining p', we correct the pressure by adding $\alpha p'$ to the old pressure value. Depending on the E-factors, the free parameter α is not necessarily set to be 1. Having obtained the pressure field, we make a shift of nodal pressures with respect to an arbitrarily referenced nodal pressure. This step is crucial to obtain a fast convergence of solutions. We then check whether the continuity constraint condition is satisfied. If not, we return to the original outer-iteration step and repeat the calculation until the convergence criterion is reached. In all the cases investigated, the

Table 1
Predicted L_2-error norms and the rates of convergence for the analytic test problem described in Section 3

Grid spacings (Δx, Δy, Δz)	Predicted L_2-error norms	
	Velocities	Pressure
2/2	0.1565E−01	0.2247E−00
2/3	0.8376E−02	0.1277E−00
2/4	0.5067E−02	0.8777E−01
2/5	0.3394E−02	0.6646E−01
2/6	0.2451E−02	0.5299E−01
2/7	0.1866E−02	0.4404E−01
2/8	0.1482E−02	0.3775E−01
2/9	0.1218E−02	0.3316E−01
2/10	0.1027E−02	0.2874E−01
Rates of convergence	1.7	1.3

solution was said to have converged when the global pressure and velocity residuals reached a value of 10^{-15}.

To formally justify the applicability of the finite volume code to investigate the channel flow details, it is customary to conduct an analysis of the incompressible Navier–Stokes equations in three dimensions. As a validation problem, we considered the problem of Eithier and Steinman [21] and conducted finite volume analyses on continuously refined grids. The predicted L_2-error norms tabulated in Table 1 led us to know that the flux discretization method applied on uniform grids provides rates of convergence for the velocity, 1.7 and the pressure, 1.3, respectively [22].

4. Results and discussion

We considered here incompressible fluid flows through symmetric channels with sudden expansion. Despite its simple geometry, this problem has served as a convenient test for the study since flow over the step shows features of more complex geometry flows, such as flow asymmetry in a symmetric channel. Fig. 1 gives an impression of the three dimensional shape of the channel. It is seen that the step of the channel is symmetrically displaced with respect to the channel centerline. This channel is characterized by an expansion ratio E ($\equiv$3), which is the ratio of the channel height, H, downstream of the expansion to the height, h, upstream, and an aspect ratio A, which is the ratio of the channel span, B, to the upstream channel height, h. The x-direction is defined as being the direction in which the bulk of the fluid travels.

A mean flow was prescribed at the channel inlet, which was upstream of the sudden expansion step with a length of 60 h. The fluid under investigation flowed through a 1 : 3 symmetric expansion into a larger straight channel, which had a length of 80 h. With the objective of studying the side wall effect on the flow asymmetry observed downstream of the step, we considered in this study 14 aspect ratios A = 3, 3.5, 3.75, 4, 5, 6, 7, 8, 9, 10, 12, 18, 24, and 48. For a better understanding of the expansion flow behavior, we also considered Reynolds numbers $Re = 60$ and 140 for the two-dimensional analyses and 60 for the three-dimensional analyses. We conducted calculations in the full domain, which consisted of a streamwise length $L_x = 140h$, including an inlet section $L_i = 60h$ prior to the sudden

Table 2
Grid details for conducting the two-dimensional grid-independence study

Grid	$N_{\Delta x}$		Δx	$N_{\Delta z}$	Δz
	Upstream	Downstream	(min, max)		(min, max)
A	15	20	(0.43, 22.0)	15	(0.25, 0.58)
B	21	29	(0.30, 15.0)	21	(0.15, 0.43)
C	30	40	(0.20, 11.0)	33	(0.10, 0.26)
D	39	51	(0.10, 9.0)	45	(0.06, 0.20)
E	47	63	(0.06, 8.0)	57	(0.04, 0.18)
F	47	93	(0.04, 5.0)	69	(0.02, 0.16)

expansion, a vertical height $L_z = 3h$ and spanwise widths $L_y = 3 \sim 48h$. For this study, non-uniform mesh distributions were used, with finer grid spacings near the step and in the vicinity of no-slip walls. Six continuously refined grids (Grid-A, Grid-B,..., Grid-F) are considered and are detailed in Tables 2 and 3.

To ensure that the solutions computed on grid spacings described above are sufficient to predict real flow physics, it is common practice to conduct grid-independent test. This three-dimensional test is impractical and is, in fact, beyond our ability since it involves a significant use of computer time. Thus, grid-independent tests were conducted in the two-dimensional context using meshes tabulated in Table 2. In the subsequent discussion of grid-independent results, it is instructive to confirm the validity of the code by considering first the Reynolds number $Re = 60$. This value falls within the range characterizing unsymmetric flow in a channel with $E = 3$ [5]. Previous experimental study revealed that laminar flow remains symmetric at $Re = 26$. As the Reynolds number is increased up to 35, no symmetric flow was observed in the channel with $E = 3$. In this grid-independent study, the problem was first solved on coarser grids. This was followed by determining whether more grid points were needed; then, an improved mesh is generated. This process was repeated until the required level of accuracy was achieved. As is apparent from Fig. 2a, that solutions computed on Grid-F compare very favorably with the experimental data [5]. Due to lack of space, we only plot in this grid-independent study velocity profiles at streamwise locations which are near the end of roof and floor eddies, $x = 7$ in Fig. 2b and $x = 20$ in Fig. 2c. Velocities at these locations are most difficult to resolve. Through this grid refinement study, it is concluded that grid density higher than Grid-B is sufficient to provide an accurate prediction.

We plot Fig. 3 to illustrate the flow asymmetry by showing that flow near the channel roof increases in velocity at the expense of the velocity in the vicinity of the channel floor. As a

Table 3
Grid details in the y-direction for the three-dimensional study

Aspect ratio A	$N_{\Delta y}$	Δy (min, max)	Grid
3	30	(0.10, 0.28)	C
3.5	30	(0.10, 0.35)	C
3.75	30	(0.10, 0.38)	C
4	30	(0.10, 0.42)	C
5	36	(0.10, 0.44)	C
6	40	(0.10, 0.49)	C
7	40	(0.10, 0.60)	C
8	40	(0.10, 0.72)	C
9	40	(0.10, 0.84)	C
10	40	(0.10, 0.97)	C
12	40	(0.10, 1.22)	C
18	40	(0.10, 2.00)	C
24	40	(0.10, 2.93)	C
48	60	(0.10, 4.14)	C
24	70	(0.02, 2.11)	F

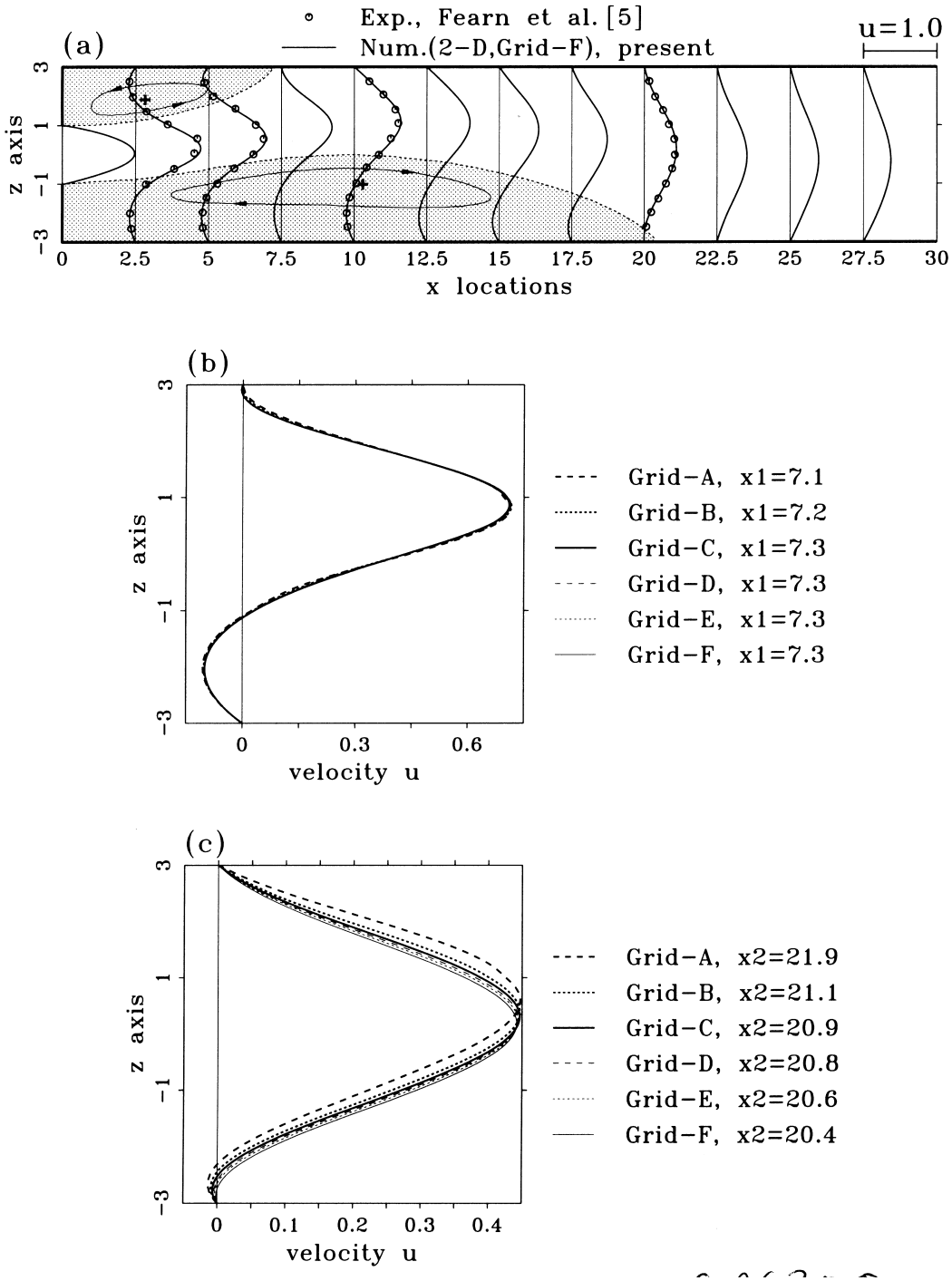

Fig. 2. (a) Comparison of two-dimensional solutions, computed on Grid-F, with the experimental data of Fearn et al. [5] for a flow with $Re = 60$ in the channel with $E = 3$; (b) Grid refinement tests for velocities plotted at $x = 7$; (c) Grid refinement tests for velocities plotted at $x = 20$.

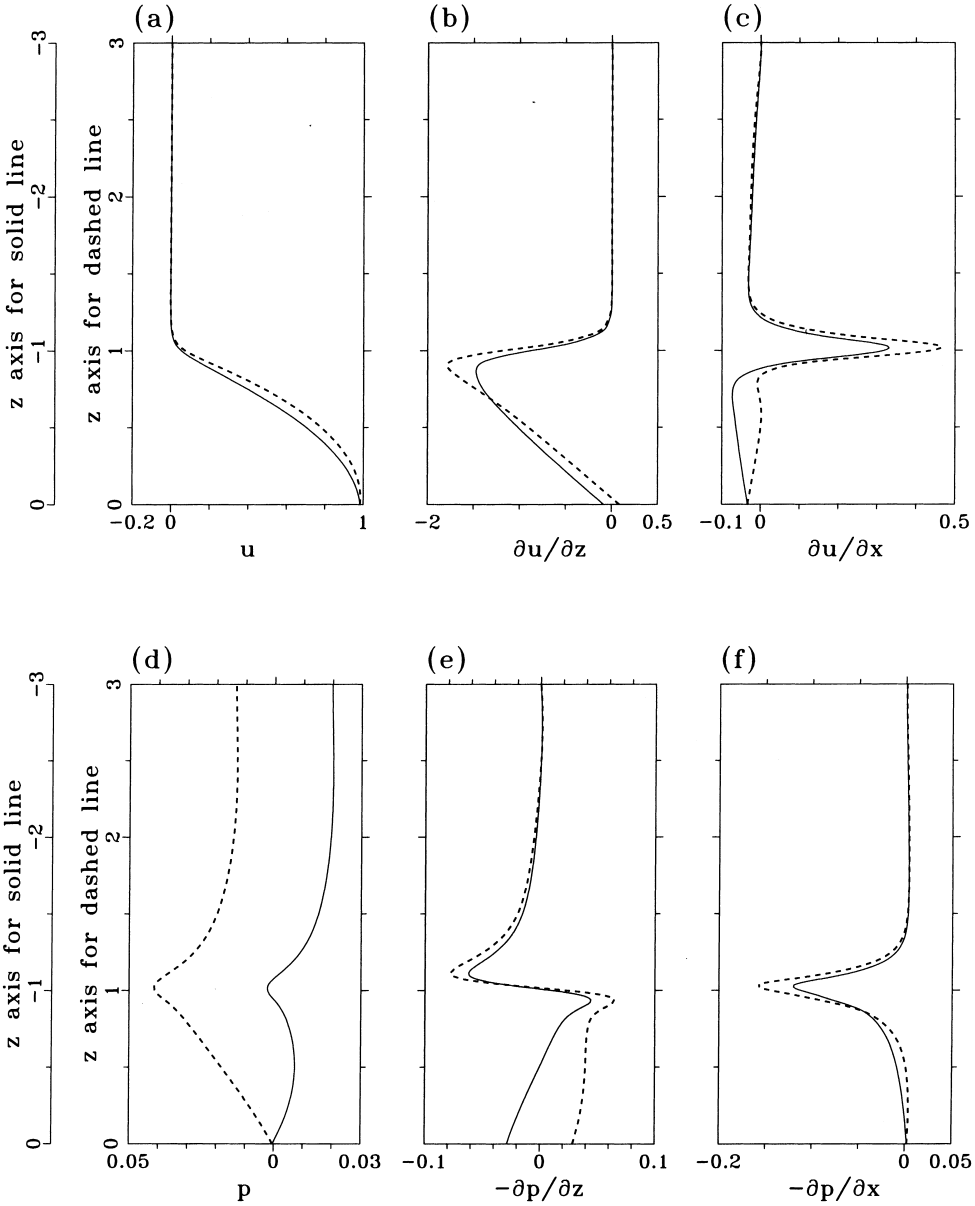

Fig. 3. Computed two-dimensional solutions plotted at the streamwise location $x = 0.1$ for the case $Re = 60$ and $E = 3$ for illuminating the Coanda effect. Solid line is for the solutions plotted in $(0.1, -3 \le z \le 0)$ and the dashed line is for the solutions plotted in $(0.1, 0 \le z \le 3)$. Solutions are computed on the Grid-F and are plotted against z-axis for: (a) u; (b) $\partial u/\partial z$; (c) $\partial u/\partial x$; (d) p; (e) $-\partial p/\partial z$; (f) $-\partial p/\partial x$.

result of the Coanda effect shown in Fig. 2a, fluid flows have higher velocity (Fig. 3a) and, thus, lower pressure (Fig. 3d). Under the circumstances, the asymmetric flow can be stably maintained by the cross-channel pressure gradient. In 1986, Sobey and Drazin [2] theoretically confirmed that the symmetric flow loses stability to one pair of asymmetric solutions. In other words, the flow undergoes a symmetry-breaking bifurcation. The flow immediately downstream of the two-dimensional step is characterized by two primary counter-rotating vortices. As a result of two primary recirculating eddies, the flow near the step corner is manifested by having large gradients both in velocity (Fig. 3b and c) and pressure (Fig. 3e and f). We then provide more numerical evidence of the Coanda effect through use of two-dimensional results for

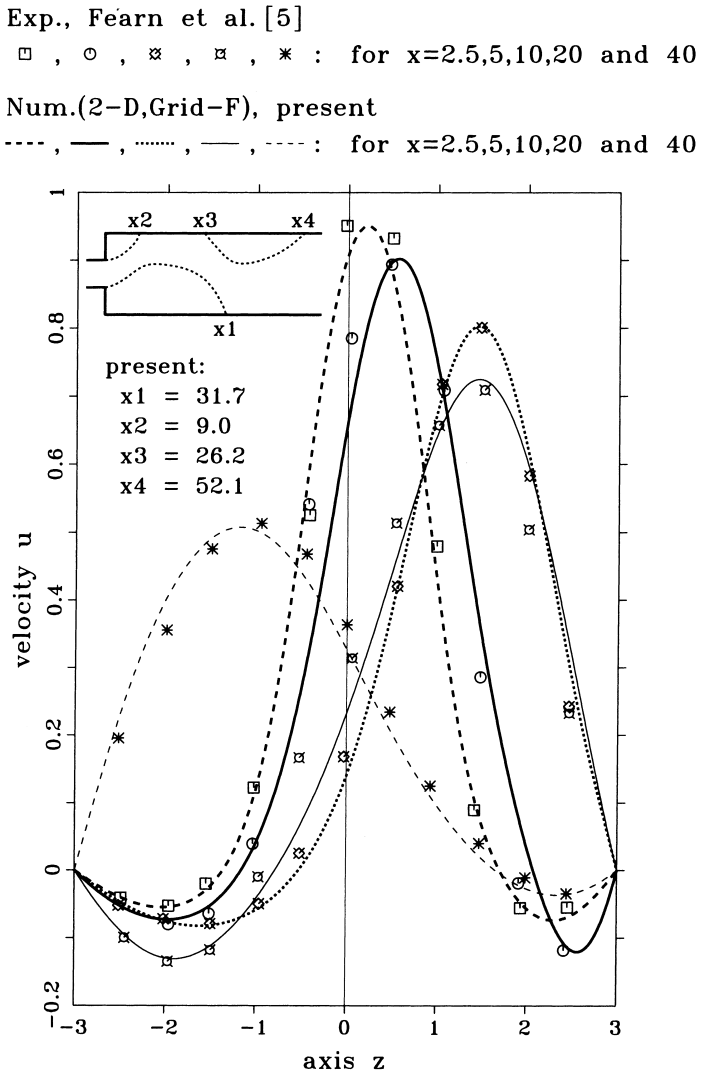

Fig. 4. Comparison of velocity u, computed on the Grid-F, with the experimental data of Fearn et al. [5] at streamwise locations $x = 2.5$, 5, 10, 20, and 40 for the Reynolds number $Re = 140$ and $E = 3$.

$Re = 140$, computed on the Grid-F. As Fig. 4 shows, agreement with the experimental data of Fearn et al. [5] is rather good, revealing that the flow asymmetry indeed exists in the symmetric channel. In the rest of this paper, we present the results, using the finest grid Grid-F, for $A = 24$, $E = 3$ and $Re = 60$. Besides this three-dimensional validation case, we also consider different aspect ratios ($3 \leq A \leq 48$) in the three-dimensional calculations on coarser grid, Grid-C. In contrast to the large number of two-dimensional solutions [4–7,10,12,14], few solutions to the three-dimensional equations governing channel flows have been performed [9,23]. This motivated the present three-dimensional study.

Before discussing three-dimensional results, the validation study was undertaken in order to allow comparison of the present results with the experimental results of Fearn et al. [5], so as to provide a measure of accuracy of the present mathematical model. As is evident from Fig. 5, agreement is rather good for the flow with $Re = 60$. We also present in Fig. 6 the convergence history for this validation study to show that three-dimensional solutions presented in Fig. 5 have perfectly converged. Three stages of different convergence nature of the error reduction are also shown in this figure.

A difficult problem which was encountered while performing three-dimensional flow simulations was the enormous amount of data generated. Care must be appropriately taken in

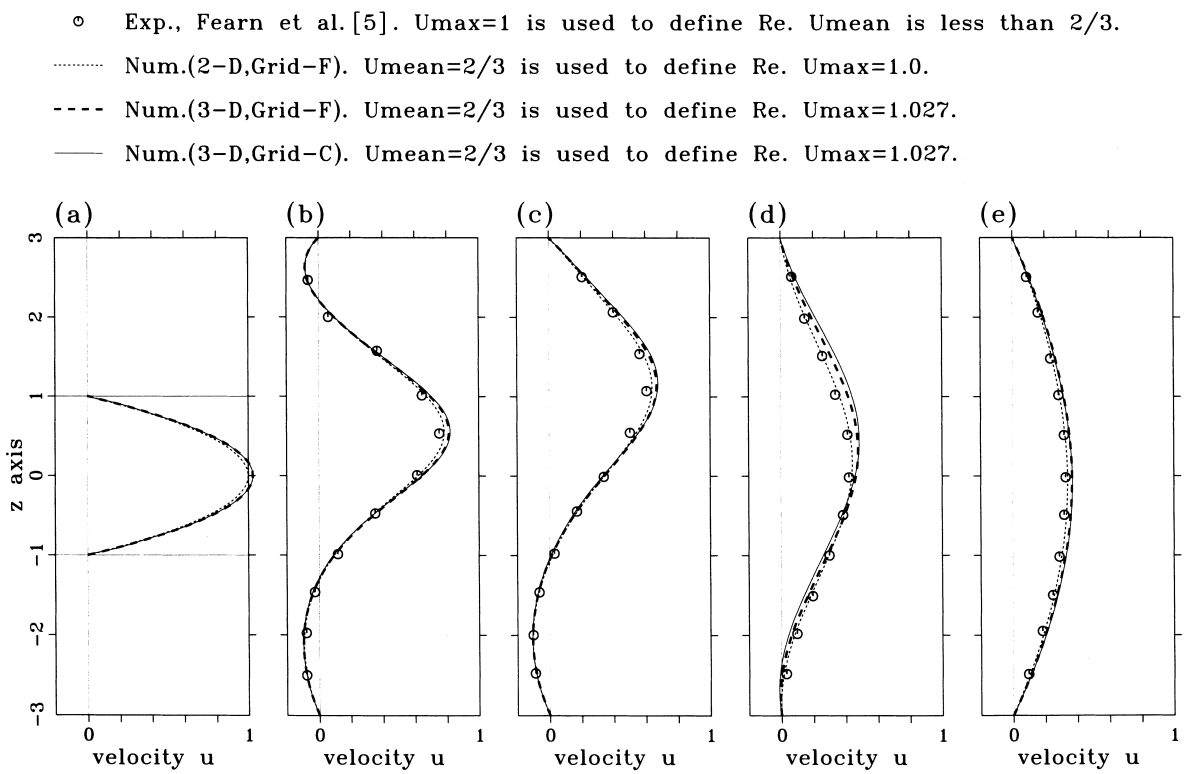

Fig. 5. Comparison of u-velocity distributions at different streamwise locations for the solutions computed on Grid-C and Grid-F: (a) $x = -5$; (b) $x = 5$; (c) $x = 10$; (d) $x = 20$; (e) $x = 40$. All solutions were obtained for $Re = 60$, $E = 3$ and $A = 24$.

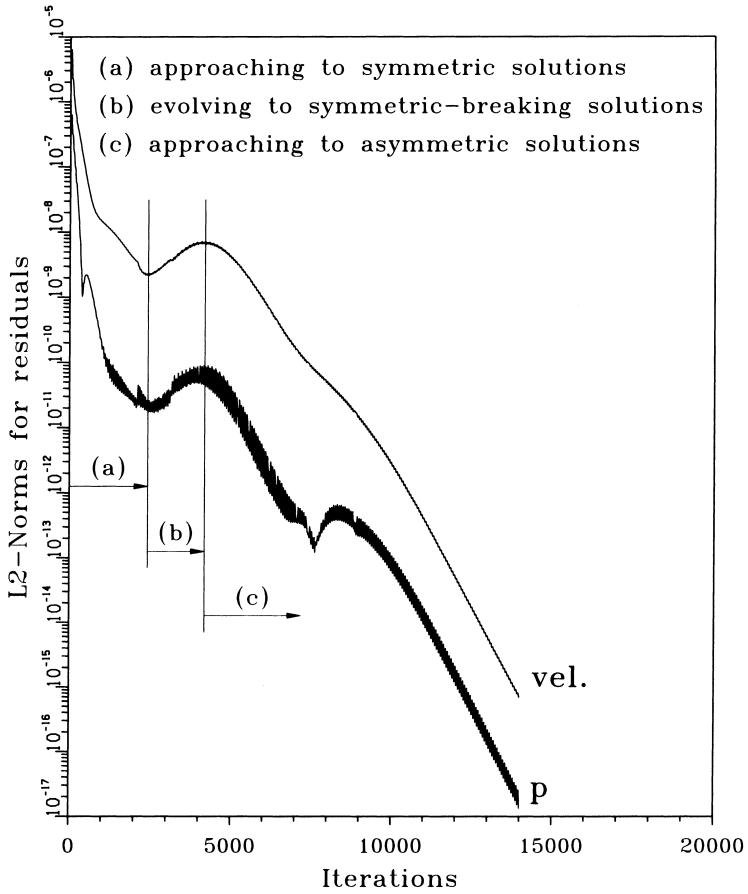

Fig. 6. Convergence history plots for the three-dimensional case with $Re = 60$, $E = 3$, and $A = 24$ on Grid-F.

order to extract meaningful flow physics and, then, obtain a profound understanding of the flow structure. This is a tedious task to conduct unless a theoretically rigorous method can be adopted. In the literature, it is found that we can conduct a topological study of limiting streamlines [24] and skin-friction lines [25] to achieve the goal. In this study, limiting streamlines which are, by definition, streamlines passing very close to the wall surface were chosen as our vector fields to gain physical insight into the pertinent fluid flows. As the topological theory states, limiting streamlines tend to diverge from lines of attachment [26]. The converse of lines of attachment is lines of separation. To lines of separation, neighboring streamlines tend to converge. We make use of the kinematic aspect of limiting streamlines to classify singular points, such as nodes, foci, and saddles. This helps depict the flow structure inferred from three-dimensional data. The plot of these singular points, supplemented with lines of separation and attachment, can provide us additional flow details.

In light of the topological theory briefly described above, we have plotted limiting streamlines on the roof, floor, step plane and vertical side wall for the channel with $A = 24$ and $Re = 60$. Fig. 7 plots the limiting streamlines, from which one can clearly observe lines of

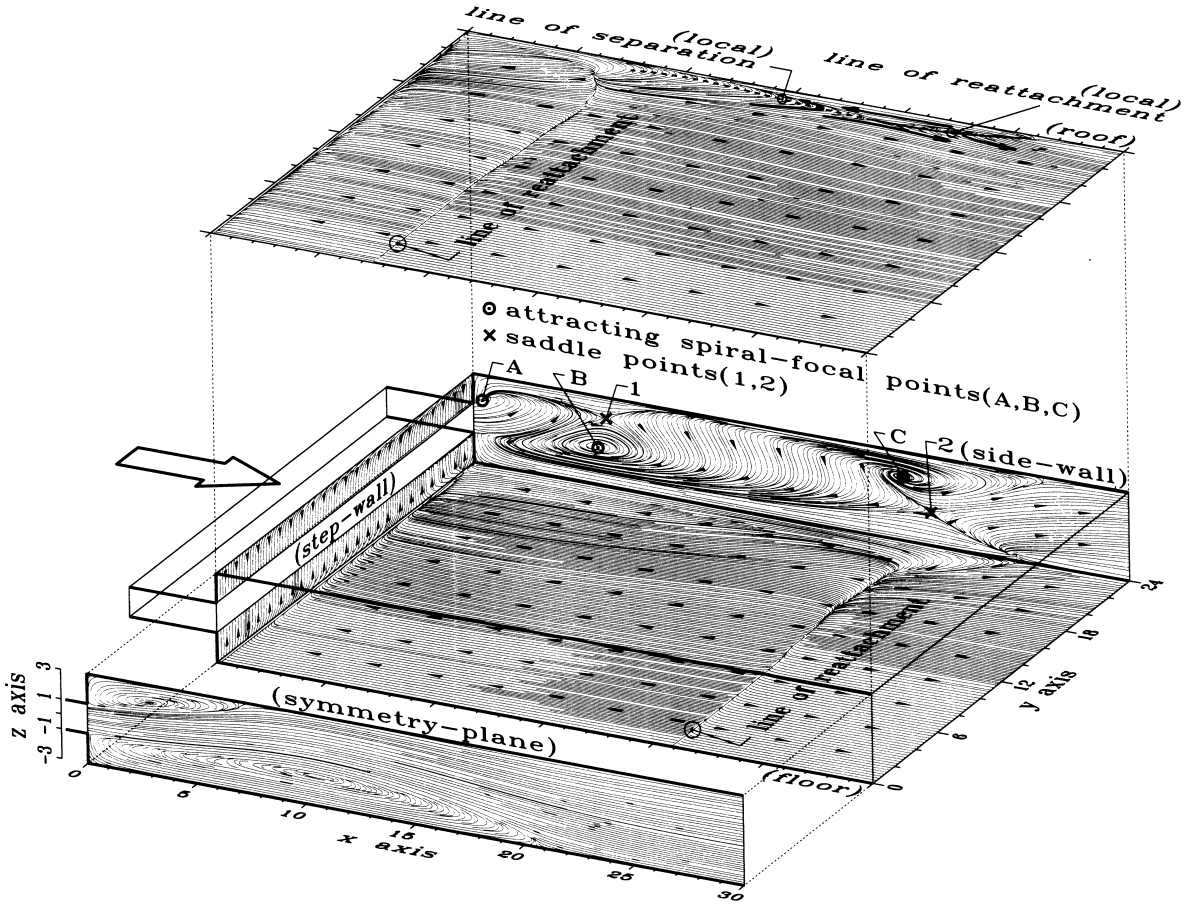

Fig. 7. Three-dimensional illustration of surface flow topology (critical points and lines of reattachment) and pseudo-streamlines on the plane of symmetry from velocities computed on Grid-F. The flow condition is for $Re = 60$ in the channel with $A = 24$, $E = 3$.

reattachment on the channel roof and floor. A characteristic feature of limiting streamlines on the roof and floor is that they are seemingly invariant with y, except in regions near the vertical side-wall. Fig. 7 also sheds some light on the flow complexity at the vertical side wall. Two saddle points, marked by '1' and '2' are shown in the downstream locations near the roof and floor reattachment, respectively. Saddle points '1' and '2' are indicative of the termination of spiral motion due to spiral motions centered at 'A' and 'B', respectively. The first saddle, below which there is a focal point 'B', is found near the channel roof. Downstream of the first saddle, there exists a much weaker singular point, '2', whose classification is similar to the first one. This saddle point is found in a streamwise location near the reattachment line. Above the saddle point '2', there also shows a spiral focal point 'C'. Emanating from the attracting spiral focal point 'A' is the vortical core line which is within the range of roof eddy. The second vortical core line originates from the attracting spiral focal point 'B'. The presence of singular point 'C' is particularly noteworthy. This critical point is present due to the vertical side-wall

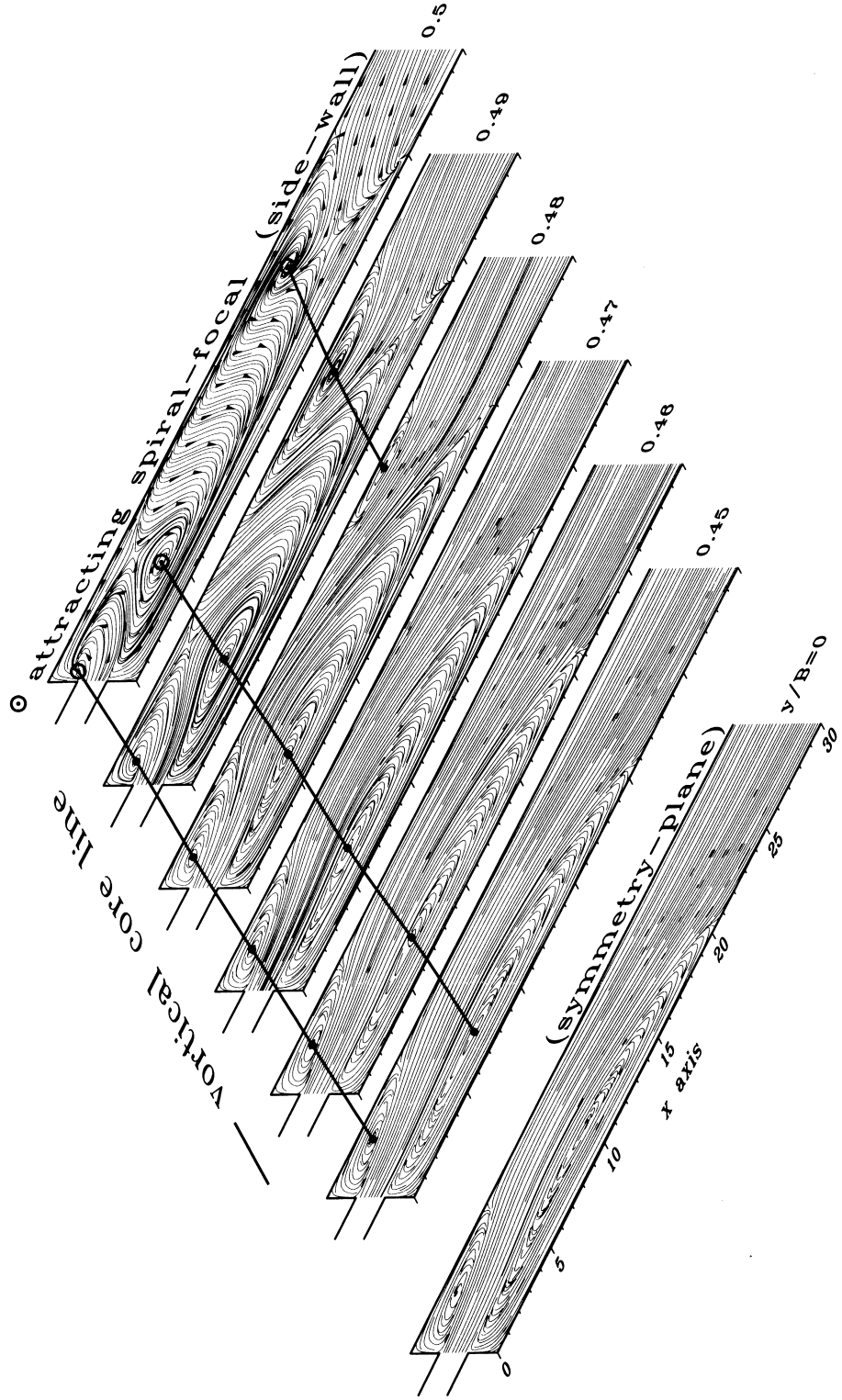

Fig. 8. Three-dimensional flow pattern, computed on Grid-F, plotted at different y planes for $Re = 60$ in the channel with $A = 24$ and $E = 3$.

and are, thus, of local nature. Near the side-wall, lines of separation and reattachment are also observed on the channel roof.

The three-dimensional nature of the flow can be best depicted by plotting u–w pseudo-streamlines in planes parallel to the side-wall plane. As Fig. 8 shows, the flow is nominally two-dimensional, except in the range of $0.45B \leq y \leq 0.5B$ where boundary layer phenomenon prevails. Owing to this side-wall boundary layer, shear force resists fluid particles to proceed to the side wall. The resulting secondary flow arises through a complex interaction between the curved flow, as manifested by the presence of primary eddies formed immediately behind the step, and the boundary layer developed over the vertical side wall. It is important to address that there exists a roof eddy in the vicinity of the vertical side-wall. This roof eddy corresponds to the spiral-focal point 'C' shown in Fig. 7. The secondary eddy is not found in the two-dimensional analysis and is too weak to extend its influence into the whole span of the expansion channel characterized by $E = 3$ and $A = 24$. The side-wall boundary layer poses shear drag on the primary motion of the fluid particles behind the step. This results in pressure gradients along the y-direction and, in turn, an increasingly large v-velocity component. It is this non-zero v-velocity component that causes the particle to move spirally with respect to the vortical core line shown in Fig. 8. This explains why particles shown in Fig. 9 proceed towards the symmetry plane $y = 0$. To show the longitudinal secondary flow induced by the vertical side-wall, we show in Fig. 10 streamline plots at selected x-planes downstream of the step plane. An important feature worth noting in the close-up plot of side-wall topology is the change of sign in the w-velocity component downstream of the spiral-focal point. Such a nature of the flow topology gives rise to longitudinal vortices, as clearly seen in the figure. The

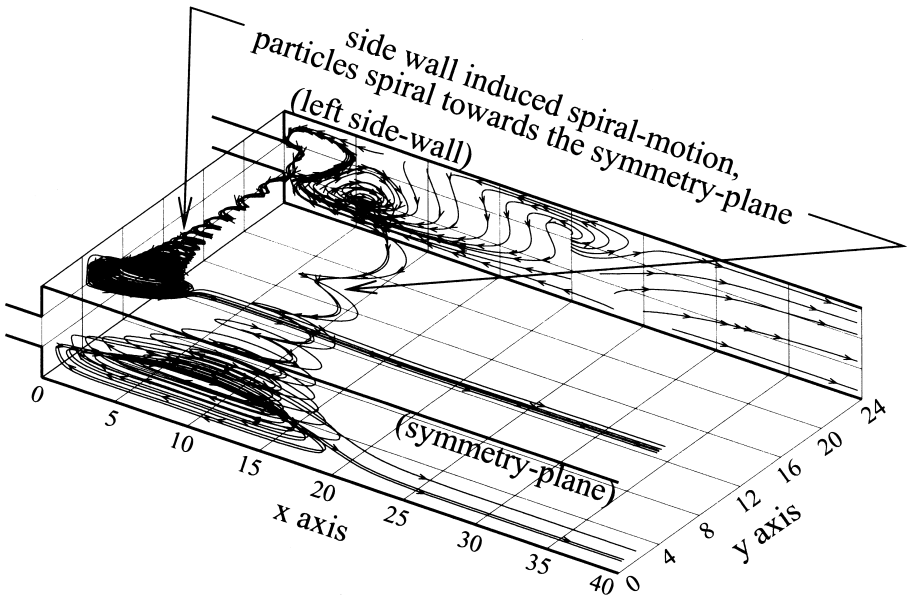

Fig. 9. Illustration of the side-wall induced particle motions spiralling towards the plane of symmetry. The side-wall surface topology is also included for the flow with $Re = 60$ in the channel with $A = 24$ and $E = 3$.

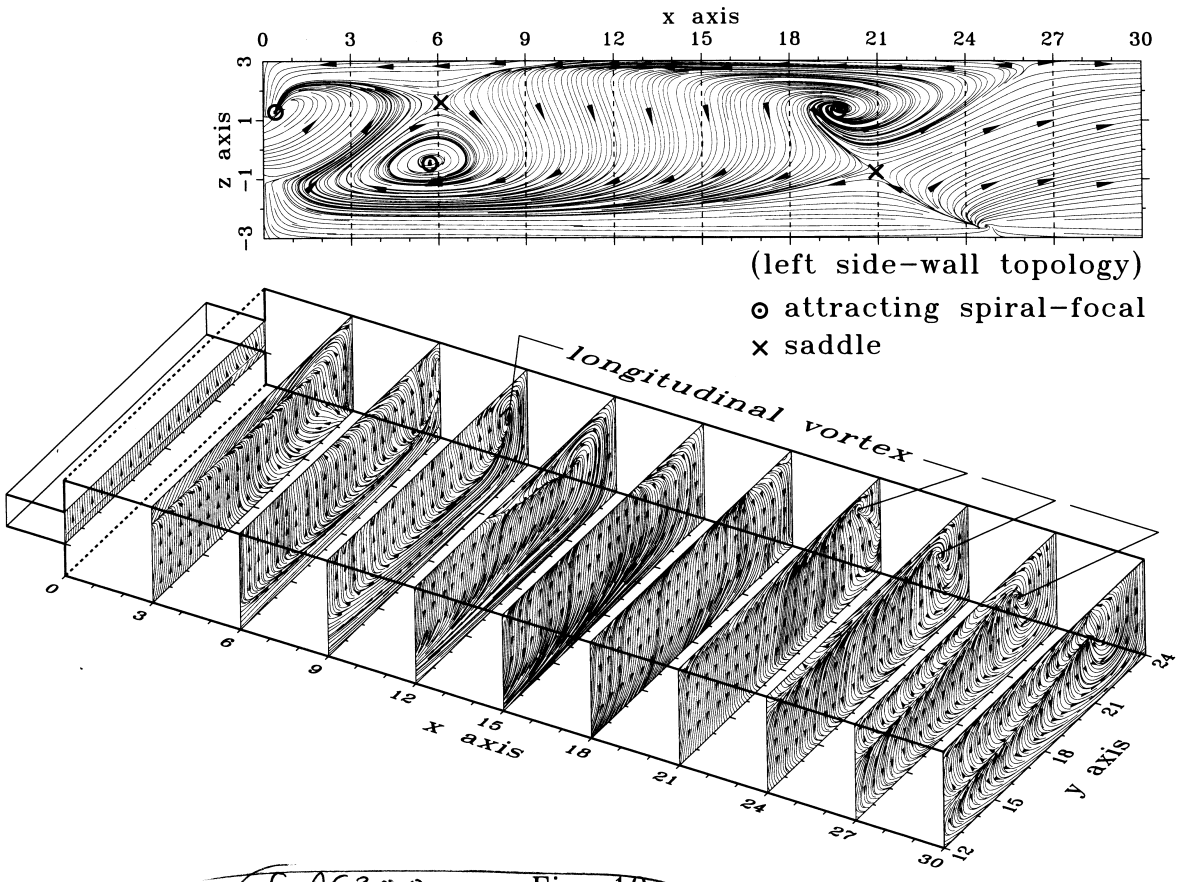

Fig. 10. Three-dimensional plot of pseudo-streamlines, computed on Gird-F, at different streamwise planes for showing the longitudinal secondary flow for $Re = 60$ in the channel with $A = 24$ and $E = 3$. The side-wall limiting streamlines are plotted for the illustration purpose.

longitudinal secondary flow is more clearly illustrated by the velocity vector plots shown in Fig. 11.

To justify the legitimate use of Grid-C in the rest of 14 three-dimensional calculations for different aspect ratios, we made a comparison of results computed from Grid-C and Grid-F with the experimental data of Fearn et al. [5] for the flow with $Re = 60$ and the channel with $A = 24$ and $E = 3$. Fig. 5, which plots the $u(z)$ distribution at different streamwise locations, shows good agreement between numerical and experimental solutions. Much less CPU times ($\mathrm{CPU}|_{\mathrm{Grid-F}}/\mathrm{CPU}|_{\mathrm{Grid-C}} \approx 15$) can be saved without loss of prediction accuracy. In Fig. 12, velocity profiles are plotted on the symmetry plane for channels with aspect ratios $A = 3$, 6, 12, 24 and 48. It is found from the figure that the two-dimensional results are strikingly different from the three-dimensional results in cases when $A < 12$. The main difference is due to characteristic velocity ($3/2u_{\max}$) used in defining Reynolds numbers for two- and three-dimensional flow problems ($u_{\max} = 1$ in two-dimensional and $u_{\max} > 1$ in three-dimensional problems). The readers are referred to Table 4, which tabulates the ratio $u_{\max}/\frac{3}{2}u_{\mathrm{mean}}$ against B

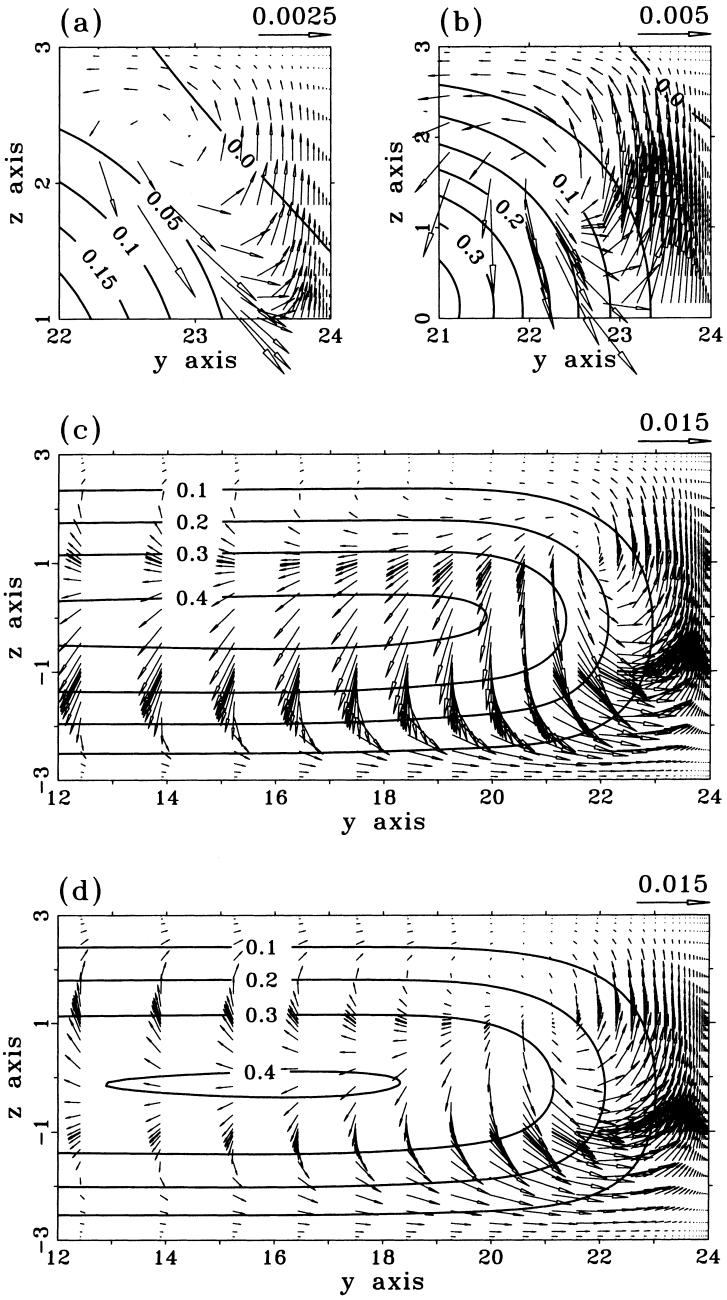

Fig. 11. *v*-*w* velocity vector and *u*-contour plots for flow $Re = 60$, computed on Grid-F, at different streamwise planes of the channel with $A = 24$ and $E = 3$: (a) at $x = 21$ plane; (b) at $x = 24$ plane; (c) at $x = 27$ plane; (d) at $x = 30$ plane.

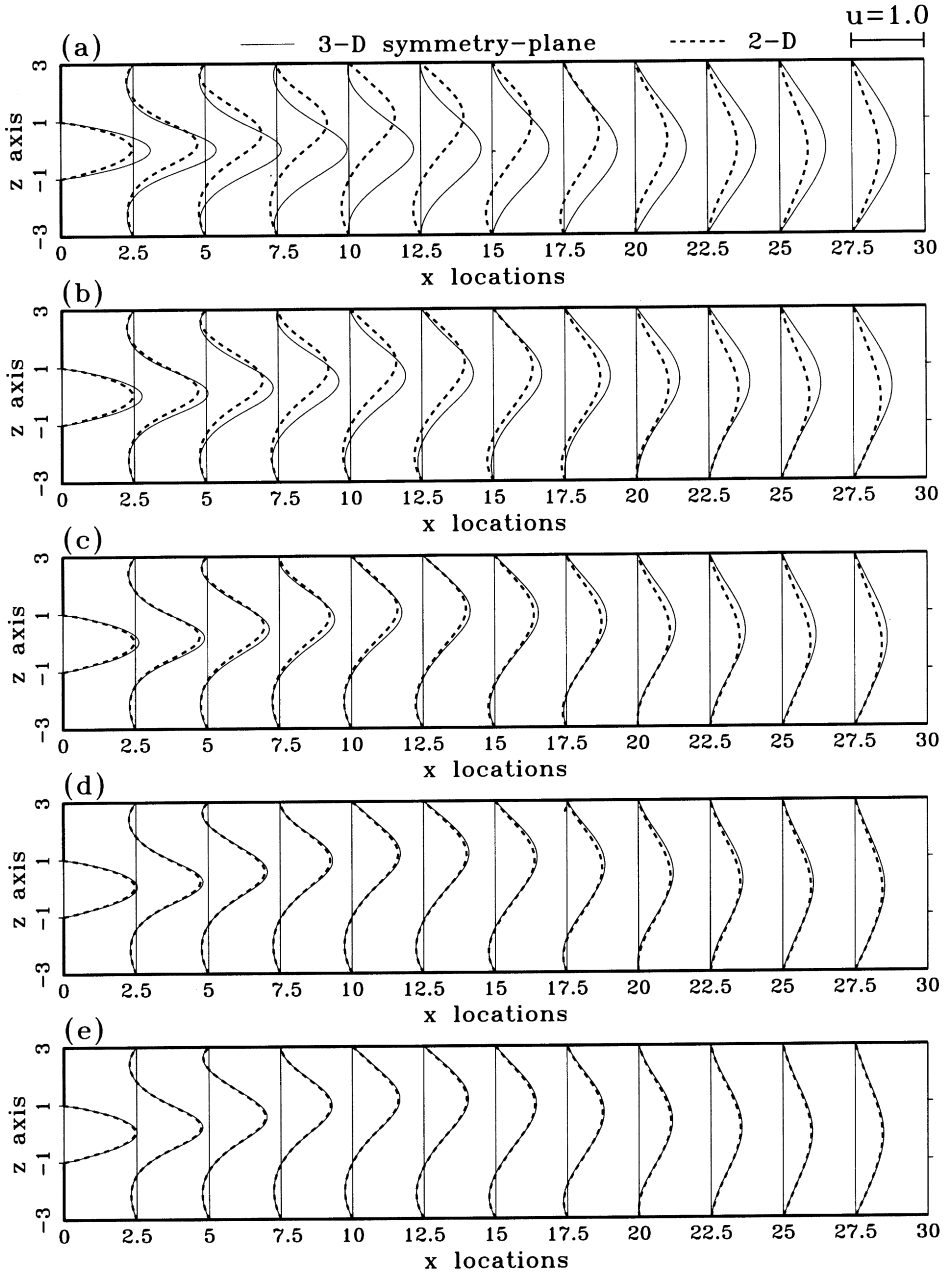

Fig. 12. Comparison of u-velocity profiles at the plane of symmetry computed from two- and three-dimensional analyses for the flow condition $Re = 60$ in the channel with $E = 3$ and different aspect ratios: (a) $A = 3$; (b) $A = 6$; (c) $A = 12$; (d) $A = 24$; (e) $A = 48$. All calculations were conducted on Grid-C.

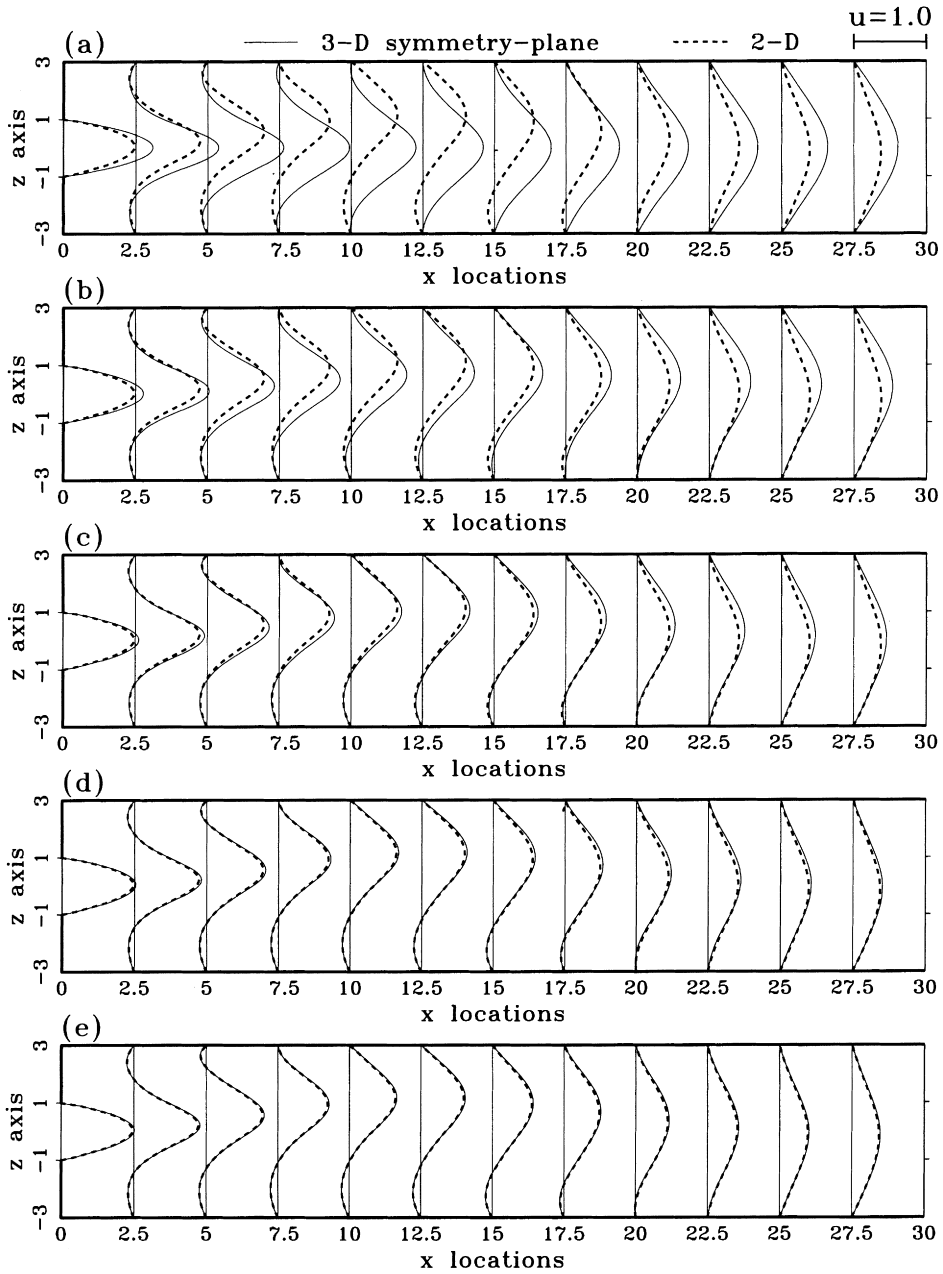

Fig. 13. Pseudo-streamlines plotted on the symmetry plane in channels with $E = 3$ and different aspect ratios: (a) $A = 3$; (b) $A = 6$; (c) $A = 12$; (d) $A = 24$; (e) $A = 48$; (f) 2D. All solutions were obtained on the Grid-C for the flow with $Re = 60$.

Table 4
The computed ratios of $u_{max}/\frac{3}{2}u_{mean}$ in the upstream channels with different aspect ratios

Aspect ratio, A	Ratio of $u_{max}/\frac{3}{2}u_{mean}$
3	1.242
3.5	1.209
3.75	1.195
4	1.182
5	1.143
6	1.117
7	1.099
8	1.086
9	1.075
10	1.067
12	1.055
18	1.036
24	1.027
48	1.013

at the channel inlet. Another reason for such difference is that three-dimensional nature of the flow prevails in channels having smaller aspect ratios. This effect can be ascribed to the increasingly important end-wall shear drag. In the channel having a very large aspect ratio, say $A = 48$, the flow is essentially two-dimensional in the core region. Virtually no difference is observed between the two- and three-dimensional results shown in Fig. 12e. This is in accord

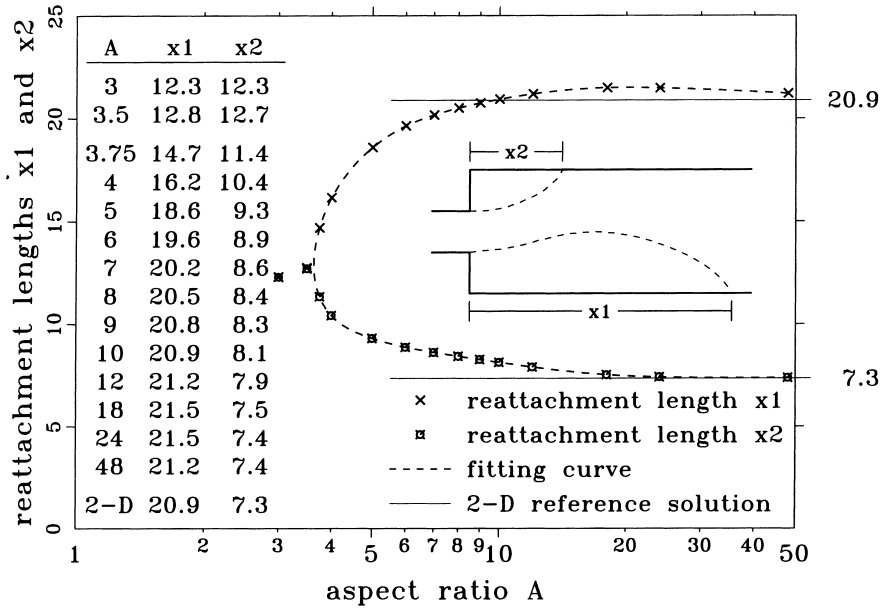

Fig. 14. Reattachment lengths x_1 and x_2 on the symmetry plane of the channel with $E = 3$ and different aspect ratios. All solutions were obtained on Grid-C for the flow with $Re = 60$.

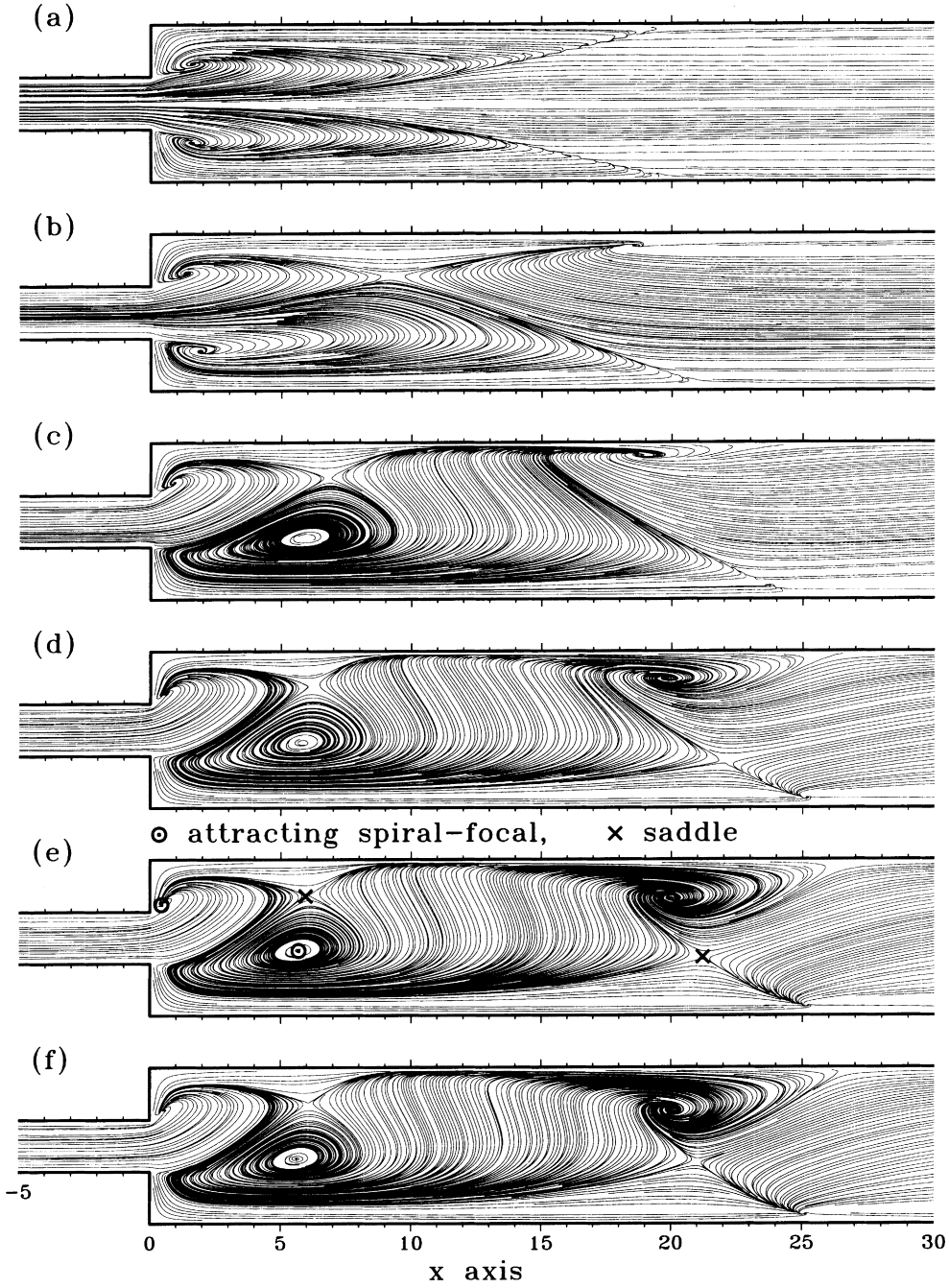

Fig. 15. The side-wall surface streaking lines in channels with $E = 3$ and different aspect ratios: (a) $A = 3$; (b) $A = 3.75$; (c) $A = 6$; (d) $A = 12$; (e) $A = 24$; (f) $A = 48$. All calculations were made on Grid-C for the flow with $Re = 60$.

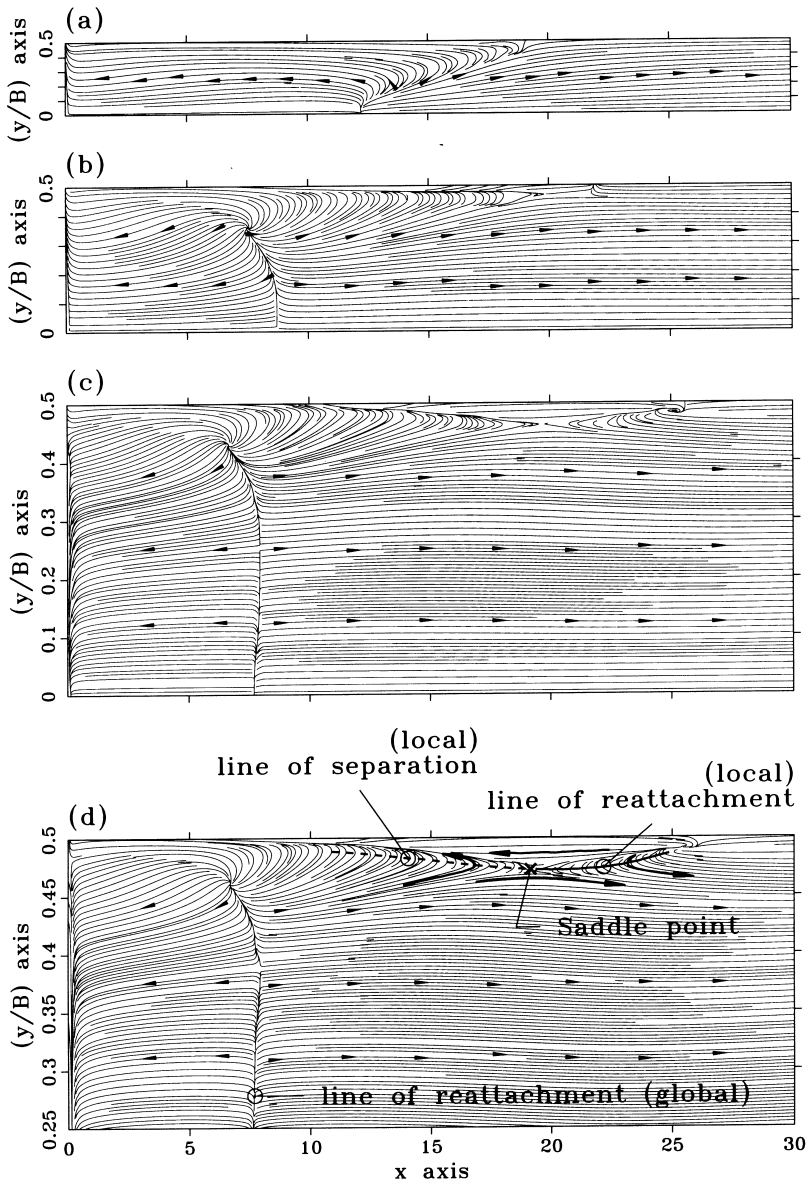

Fig. 16. The surface flow topology on the channel roof with $E = 3$ and different aspect ratios: (a) $A = 3$; (b) $A = 6$; (c) $A = 12$; (d) $A = 24$. All calculations were performed on Grid-C for the flow with $Re = 60$.

with our expectation that the flow in a channel with an infinitely large value of A can be rationally regarded as being two-dimensional.

Since flow asymmetry in symmetric channels with sudden expansions has been the subject of much attention, we were motivated to study the effect of A on the flow asymmetry for an incompressible fluid flow at $Re = 60$ and $E = 3$. Fig. 13 presents a comparison of streamlines plotted at the symmetry plane in channels with different values of A. What is now evident is

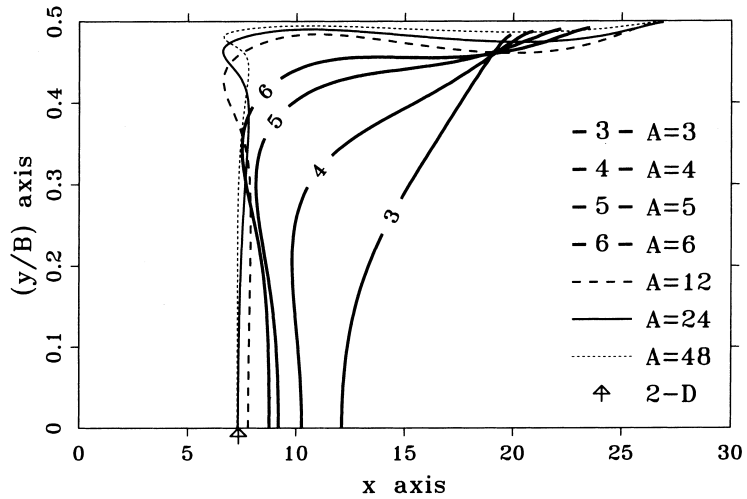

Fig. 17. Comparison of lines of reattachment on the channel roof with $E = 3$ and different aspect ratios $A = 3$, 4, 5, 6, 12, 24, 48. All analyses were carried out on Grid-C for the flow with $Re = 60$.

that flow symmetry is stably maintained when A is equal to 3. As the aspect ratio of the channel A is increased up to a value of 6, flow asymmetry becomes clearly observed. To find a critical aspect ratio, above which the flow undergoes a transition to asymmetry, we conducted three-dimensional calculations in channels with aspect ratios falling in between 3 and 6. Through numerical simulations, it is revealed from Fig. 14 that the critical aspect ratio is about 3.5. It is fair to conclude from Fig. 14 that the three-dimensional flow approaches that of the two-dimensional flow as $A > 12$.

Typical of a flow in a symmetric channel with sudden expansion is the vortical flow formed behind the step. The physical details of such flow can be explored using the underlying theory of topology. Efforts in this direction have prompted us to plot limiting streamlines at the side-wall, roof and floor of the channel. As seen from limiting streamlines plotted at the vertical side wall, the flow shown in Fig. 15 is symmetric with respect to $z = 0$ for the case of $A = 3$. This is not the case for a flow in larger aspect ratio channels. Revealed clearly by this figure is a focal-saddle pair of critical points when the channel aspect ratio is increased to 6. We will now provide details of the flow separation and reattachment in the channel roof and floor. To do so, it is instructive to apply the topological theory to theoretically determine the separation locations on the roof and reattachment locations on the roof and floor of the channel. Fig. 16 plots the limiting streamlines on the channel roof. The lines of reattachment are clearly revealed in the sense that neighboring limiting streamlines repel from these critical lines. The lines of local separation/reattachment near the side-wall are also observed as $A > 6$. For purposes of completeness, we plot in Fig. 17 lines of reattachment and separation on the channel roof. We also plot in Fig. 18, limiting streamlines on the channel floor and in Fig. 19, lines of reattachment for the sake of comparison.

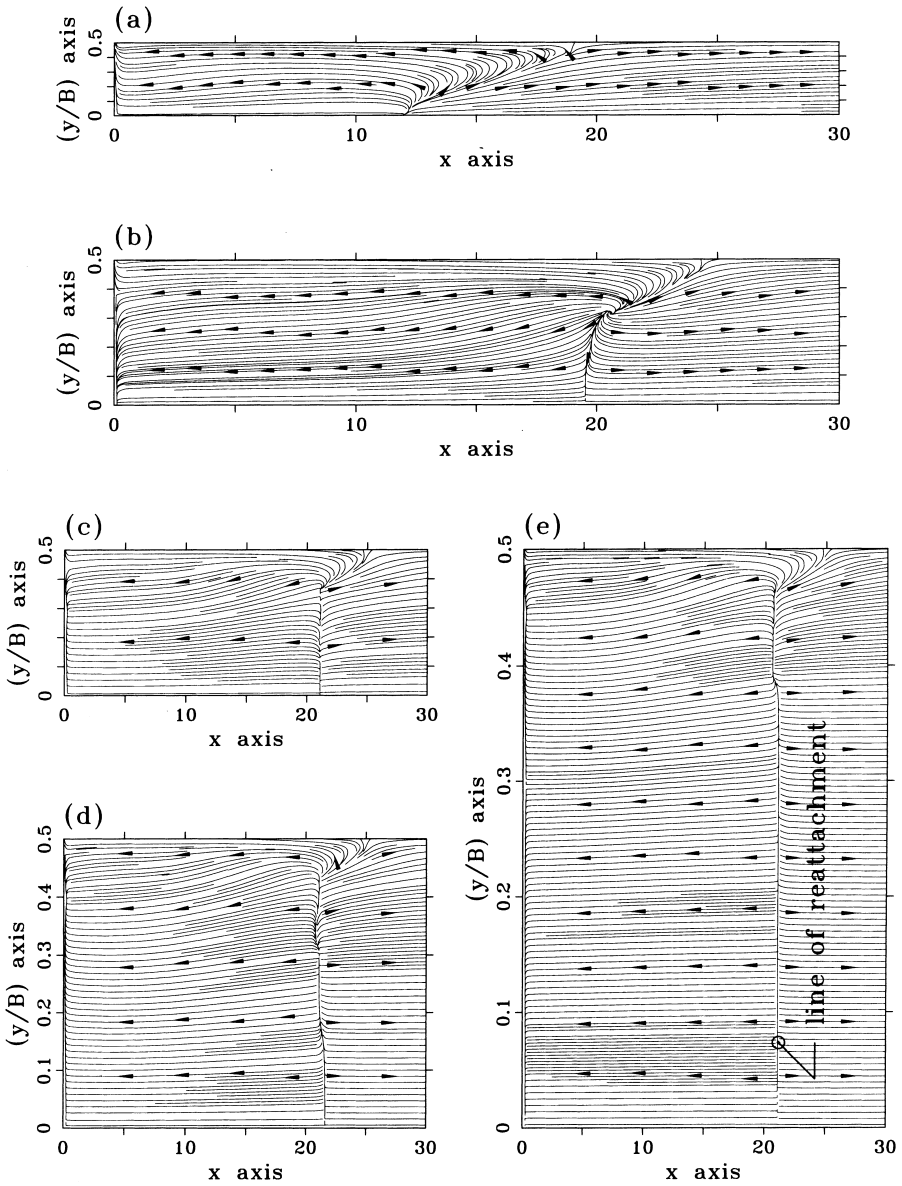

Fig. 18. The surface flow topology on the channel floor with $E = 3$ and different aspect ratios: (a) $A = 3$; (b) $A = 6$; (c) $A = 12$; (d) $A = 24$; (e) $A = 48$. All analyses were carried out on Grid-C for the flow with $Re = 60$.

5. Concluding remarks

Computational investigation into the incompressible channel flow over a symmetric sudden expansion confirms the general trends of previous two-dimensional investigations and provides further information which adds to knowledge of the three-dimensional flow structure. Consideration has been given to the critical aspect ratio, above which an initially symmetric

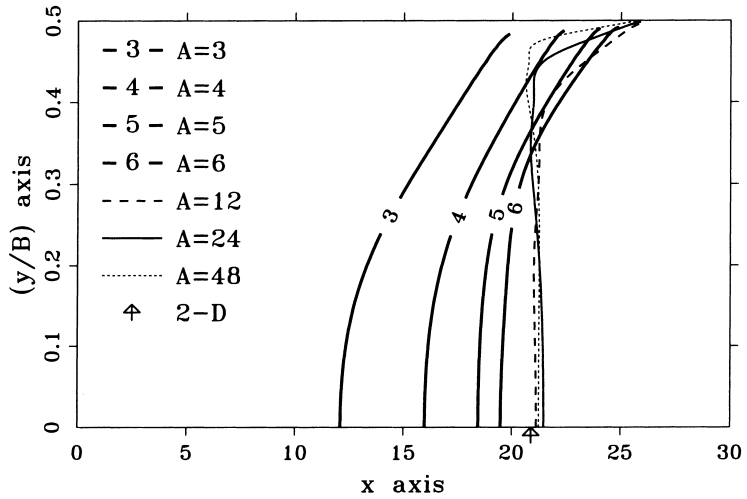

Fig. 19. Comparison of lines of reattachment on the channel floor with $E = 3$ and $A = 3$, 4, 5, 6, 12, 24, 48. All analyses were carried out on Grid-C for the flow with $Re = 60$.

flow will develop into an asymmetric flow due to the Coanda effect. Through intensive study, it has been found that flow symmetry remains a feature of the flow in channels whose aspect ratios are less than 3.5. Numerical solutions have also shown that the centerplane flow is nominally two-dimensional as the aspect ratio is larger than 12. Thanks to the theoretically rigorous theory of topology, our understanding of the flow structure has been increased through depiction of lines of separation and reattachment, critical points, such as spiral focal points and saddles. In contrast to experimental investigations, bifurcation observed is most likely to be triggered by small asymmetries in the channel geometry and flow conditions, we attribute the numerical flow asymmetry in the geometrically symmetric channel to bifurcation triggered possibly by discretization errors, asymmetry of the numerical algorithm employed to solve the basic equations of fluid flows. Another source which causes flow asymmetry to occur is due to REAL-number representation in computer [27]. In any computer hardware system, the difference between two consecutive floating-point numbers (gap, or spacing) are uneven in size. Even a negligibly small flow asymmetry may be amplified by locally high shear strain in the vicinity of a step corner.

Acknowledgements

Support for this research provided by the National Science Council of the Republic of China under Grant NSC87-2611-E002-027 is gratefully acknowledged. The authors would like to express sincere appreciation to the reviewers of this manuscript for providing important and helpful comments to improve its content.

References

[1] Wille R, Fernholz H. Report on the first European Mechanics Colloquium, on the Coanda effect. J Fluid Mech 1965;23(4):801–19.
[2] Sobey IJ, Drazin PG. Bifurcations of two-dimensional channel flows. J Fluid Mech 1986;171:263–87.
[3] Cherdron W, Durst F, Whitelaw JH. Asymmetric flows and instabilities in symmetric ducts with sudden expansions. J Fluid Mech 1978;84(1):13–31.
[4] Sobey IJ. Observation of waves during oscillatory channel flow. J Fluid Mech 1985;151:395–426.
[5] Fearn RM, Mullin T, Cliffe KA. Nonlinear flow phenomena in a symmetric sudden expansion. J Fluid Mech 1990;211:595–608.
[6] Shapira M, Degani D. Stability and existence of multiple solutions for viscous flow in suddenly enlarged channels. Computers and Fluids 1990;18(3):239–58.
[7] Drikakis D. Bifurcation phenomena in incompressible sudden expansion flows. Phys Fluids 1997;9(1):76–87.
[8] Alleborn N, Nandakumar K, Raszillier H, Durst F. Further contributions on the two-dimensional flow in a sudden expansion. J Fluid Mech 1997;330:169–88.
[9] Schreck E, Schäfer M. Numerical study of bifurcation in three-dimensional sudden channel expansions. Computers and Fluids 2000;29(5):583–93.
[10] Macagno EO, Hung TK. Computational and experimental study of a captive annual eddy. J Fluid Mech 1967;28(1):43–64.
[11] Durst F, Melling A, Whitelaw JH. Low Reynolds number flow over a plane symmetric sudden expansion. J Fluid Mech 1974;64(1):111–28.
[12] Durst F, Pereira JCF, Tropea C. The plane symmetric sudden-expansion flow at low Reynolds number. J Fluid Mech 1993;248:567–81.
[13] Armaly BF, Durst F, Pereira JCF, Schönung B. Experiment and theoretical investigation of backward-facing step flow. J Fluid Mech 1983;127:473–96.
[14] Scott PS, Mirza FA. A finite element analysis of laminar flows through planar and axisymmetric abrupt expansions. Computers and Fluids 1986;14(4):423–32.
[15] Ladyzhenskaya OA. Mathematical problems in the dynamics of a viscous incompressible flow. New York: Gordon and Breach, 1963.
[16] Harlow FH, Welch JE. Numerical calculation of time-dependent viscous incompressible flow of fluid with free surface. Phys Fluids 1965;8:2182–9.
[17] Chiang TP, Hwang Robert R, Sheu WH. Finite volume analysis of spiral motion in a rectangular lid-driven cavity. Int J Numer Meths in Fluids 1996;23:325–46.
[18] Leonard BP. A stable and accurate convective modeling procedure based on quadratic upstream interpolation. Comput Meths Appl Mech Engrg 1979;19:59–98.
[19] Patankar SV. Numerical heat transfer and fluid flow. Washington DC: Hemisphere, 1980.
[20] Van Doormaal JP, Raithby GD. Enhancements of the SIMPLE method for predicting incompressible fluid flows. Numer Heat Transfer 1984;7:147–63.
[21] Eithier CR, Steinman DA. Exact fully 3D Navier–Stokes solutions for benchmarking. Int J Numer Meth in Fluids 1994;19:369–75.
[22] Chiang TP, Sheu WH, Hwang Robert R. Effect of Reynolds number on the eddy structure in a lid-driven cavity. Int J Numer Meths in Fluids 1998;26:557–79.
[23] Baloch A, Townsend P, Webster MF. On two- and three- dimensional expansion flows. Computers and Fluids 1995;24(8):863–82.
[24] Legendre R. Séparation de courant écoulerment laminaire tridimensionnel. Rech Aéro 1956;54:3–8.
[25] Lighthill M. Attachment and separation in three-dimensional flow. In: Rosenhead, II L, editor. Laminar boundary layers, 2(6). Oxford: Oxford University Press, 1963. p. 72–82.
[26] Tobak M, Peaks DJ. Topology of three-dimensional separated flows. Ann Rev Fluid Mech 1982;14:61–85.
[27] Smith G. Writing good software in Fortran. Englewood Cliffs, NJ: Prentice Hall, 1998.